Correlation between optical properties and barrier composition in $In_xGa_{1-x}P$/GaAs quantum wells

J. Martínez-Pastor[a)]
Instituto de Ciencia de Materiales de la Universidad de Valencia, 46100 Burjassot, Valencia, Spain

L. González
Instituto de Microelectrónica de Madrid (CNM-CSIC), Isaac Newton 8, P.T.M., 28760 Tres Cantos Madrid, Spain

G. Aragón
Departamento de Ciencia de Materiales e Ingeniería Metalúrgica y Química Inorgánica, Universidad de Cádiz, Apdo. 40, Puerto Real, 11510 Cádiz, Spain

Ch. Guenaud and E. Deleporte
Laboratoire de Physique de la Matière Condensée de l'Ecole Normale Superieure, 24 rue Lhomond, 75231 Paris Cedex 05, France

(Received 21 January 1998; accepted for publication 29 August 1998)

In this work high structural and optical quality $In_xGa_{1-x}P$/GaAs quantum wells in a wide range of thicknesses have been successfully grown on GaAs substrates by low temperature atomic layer molecular beam epitaxy. We demonstrate that compositional fluctuations in the barrier alloy are responsible for the inhomogeneous broadening and spatial localization effects observed in the excitonic recombination, the influence of quantum well width fluctuations being negligible in comparison. An important change of the optical transition energies in these quantum wells is observed when tuning a 10% In–Ga ratio in the alloy around the lattice match composition ($x=0.48$). This change is related to the barrier band gap variation and the intrinsic characteristics of the InGaP/GaAs heterostructure: different exciton binding energy from tensile to compressive strain in the barrier, and a possible dependence of the conduction band offset on the In composition. © *1998 American Institute of Physics.* [S0021-8979(98)04023-7]

I. INTRODUCTION

Much work has been devoted in the last years to the growth, control, and characterization of InGaP epitaxial layers lattice matched to GaAs (see Refs. 1–3 and references therein for the state of the art). InGaP layers have been proposed as a partner of GaAs for use as a good substitute for AlGaAs in electronic and optoelectronic devices, since the latter contains a larger concentration of deep traps and has a higher reactivity with oxygen. Furthermore, this material can be the base of future light emitting diodes (LEDs) and laser diodes operating in the visible range when combined with larger band gap materials, as the promising quaternary alloy (AlGa)InP, also matched to GaAs.[4] Therefore, from InGaP cladding layers of InGaAs and GaAs based lasers to InGaP based heterostructures (heterojunction transistors, laser diodes, tandem solar cells, etc.),[5–7] this alloy has introduced new perspectives in optoelectronics, from the infrared to the visible spectral range. One can also tune the lattice mismatch (i.e., the band gap and electronic properties) between InGaP and GaAs by slightly changing the In–Ga composition ratio in the alloy, without reducing its optical quality,[8] and even induce drastic changes[9,10] if large ordering and phase separation effects (both exhibiting a periodic arrangement in the crystal) could be controlled during growth.

In a previous paper,[8] we have shown that both the GaAs well width and the In–Ga ratio in the barrier should be taken into account for optimizing the best emitting structures. This ratio not only determines the alloy band gap, but it also seems to influence the effective band alignment between the GaAs and the InGaP. In fact, we have observed an important blue shift in the photoluminescence (PL) lines of the GaAs quantum wells (QWs) confined by $In_xGa_{1-x}P$ barriers under tensile strain ($x<0.48$), with respect to identical QWs confined by $In_xGa_{1-x}P$ under compressive strain ($x>0.48$). This would mean that x can be used as an additional design parameter for InGaP/GaAs heterostructures.

In this work we extend the investigation of those samples and others grown under similar conditions, by studying and correlating their structural and optical properties. New samples with larger lattice mismatch to GaAs and also containing a higher number of QWs in the range 0.8–10 nm have been grown, in order to establish a better knowledge of the framework of the InGaP/GaAs system. It is worth noting that the InGaP alloy in all samples is nominally random in nature under the conditions used to grow them.[3]

II. SAMPLES AND EXPERIMENT

Several $In_xGa_{1-x}P$/GaAs heterostructures were grown on semi-insulating (001) GaAs substrates, either after a 350 nm thick GaAs buffer layer (type A samples) or after a mixed 500 nm thick GaAs/500 nm thick InGaP buffer layer (type B samples). The InGaP buffer layers and the hetero-

a)Electronic mail: Martinep@uv.es

structures have been grown by atomic layer molecular beam epitaxy (ALMBE) at a substrate temperature $T_s = 420\,^{\circ}\mathrm{C}$ and a growth rate of 1 monolayer per second (ML/s). The P_2 was produced in a solid source cell with a fast acting valve and cracking section. We will consider here only one sample from type B ones, that nominally lattice matched to GaAs ($x_{\mathrm{In}} = 0.48$), labeled B1. It consists of five GaAs quantum wells of nominal thicknesses: 20, 12, 6, 4 and 3 nm, separated by 50 nm thick $In_xGa_{1-x}P$ barriers; a GaAs cap layer of 4 nm ends the structure. Type A samples contain seven QWs of nominal thicknesses: 15, 7.1, 4.8, 3.4, 2.3, 1.42, and 0.85 nm, separated by 20 nm thick $In_xGa_{1-x}P$ barriers (30, 40, and 50 nm thick for the last three QWs in order to reduce wave function overlap). The nominal composition of the barriers is $x_{\mathrm{In}} = 0.53$ and $x_{\mathrm{In}} = 0.43$ for samples A1 and A2, respectively.

The optical experiments have been carried out in the temperature range 2–300 K. The continuous wave PL and PL excitation (PLE) measurements have been performed by using either an Ar^+ pumped Ti:sapphire laser (700–820 nm) or a 1000 W Xe lamp (before a double $\frac{1}{4}$ m monochromator) as excitation sources. The optical excitation density on the samples was kept typically below 10 W/cm^2 for both kind of excitation sources; we note that the illuminated area of the sample after focusing the beam coming from the Xe lamp excitation system is about 100 times larger than that obtained after focusing the Ti:sapphire laser beam. The PL signal was dispersed through a 100 cm double-grating monochromator (giving a spectral resolution in our PL experiments below 0.2 meV) and detected with a cooled GaAs photomultiplier by a standard lock-in technique. Given the limited wavelength range of the Ti:sapphire laser, the Xe lamp has been used to perform the PLE spectra of the different QWs around the band edge of the InGaP barrier and also for narrow QWs (below 3 nm). With the Xe lamp setup, the heavy hole (HH) exciton resonance in PLE cannot be well resolved from stray light without compromising the PL signal. In this way, two kinds of PLE spectra have been measured for narrow QWs: (i) PLE detected at the PL peak energy and (ii) PLE detected at an energy sufficiently below the PL peak to resolve the HH–exciton resonance. In type (i) spectra we obtain well defined LH–exciton resonances. In type (ii) the spectra are noisy with broader LH(HH)–exciton resonances, leading to imprecise HH peak energies (~5–10 meV) for the three thinnest QWs in samples A1 and A2.

Structural characterization has been performed by high resolution x-ray diffraction (four Ge crystal monochromator in the primary optics and a single Ge crystal analyzer) and transmission electron microscopy (TEM) in order to make a correlation with the optical properties of our InGaP/GaAs heterostructures. The samples, both for cross-section and plan-view TEM, were thinned by mechanical polishing and Ar^+ ion milling. The TEM observations were performed on a JEOL 1200EX microscope at an accelerating voltage of 120 kV.

III. STRUCTURAL CHARACTERIZATION

Figure 1 shows a $\Omega/2$ scan of the (004) reflection for sample A1. A dynamical simulation (see dotted line in Fig. 1) has been carried out in order to reproduce the experimental x-ray diffraction pattern in all samples. The most important parameter in this simulation is the In composition of the $In_xGa_{1-x}P$ barriers. The best fitting values give: $x_{\mathrm{In}} = 0.467 \pm 0.003$, $x_{\mathrm{In}} = 0.541 \pm 0.006$ and $x_{\mathrm{In}} = 0.427 \pm 0.003$ for samples B1, A1, and A2, respectively. These values represent a deviation from nominal values (those given in Sec. II) of less than 3%, 3%, and 1% in samples B1, A1, and A2, respectively. The thicknesses of the barriers and QWs are also included in the simulation and give a rather complicated interference pattern (see dotted line in Fig. 1). However, a variation of these parameters to find the best fit to the experimental spectra cannot be done successfully in all cases because the experimental interference pattern (see the low intensity features of the experimental spectrum in Fig. 1) does not offer the desired information. In any case, the good agreement between nominal and experimental values for the alloy composition assures a correct calibration of the growth rate, both for InGaP and GaAs layers in the structure. Therefore, we can assume that the total thickness of the QWs grown in each sample deviates from the nominal value around the same quantity measured for the alloy composition (3%). This means that the nominal thickness for every QW in our samples is a good value for a correct interpretation of the observed optical properties. The error in the total thickness of the QWs (a few GaAs monolayers, 1 ML = 0.283 nm) can be related to a rather low interface roughness (mainly in the thinnest QWs: 3, 5 and 8 ML thick ones in samples A1 and A2) better than large size islands or a 1–2 ML change in the thickness of the QW (more probable in QWs thicker than 10 nm).

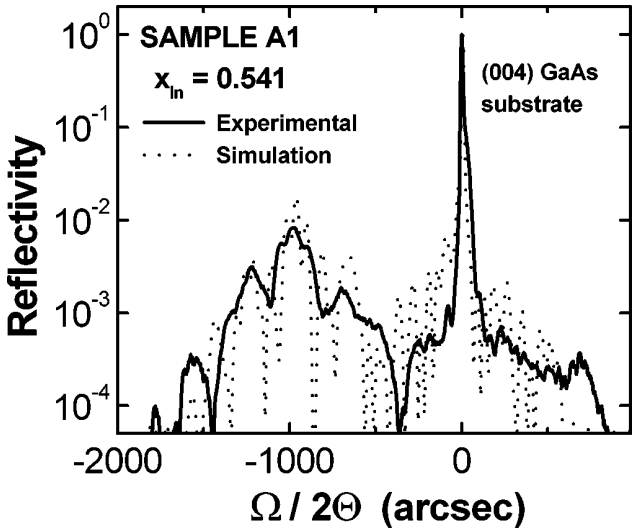

FIG. 1. High resolution x-ray $\Omega/2\vartheta$ scan of the (004) reflection for sample A1 ($x_{\mathrm{In}} = 0.541$). The simulated diffractogram is also shown.

Another key point for understanding the excitonic recombination in InGaP/GaAs QWs is the origin of the inhomogeneities giving rise to the PL broadening at low temperatures. With this aim, structural characterization by TEM was also performed both in planar view and cross section. All the QWs exhibit nearly flat interfaces (within the accuracy given

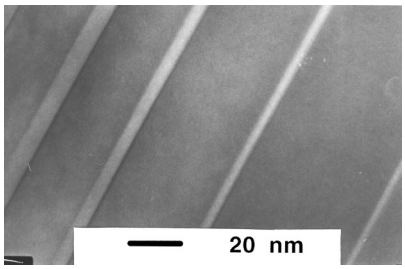

FIG. 2. Cross-section image of sample A2 ($x_{In}=0.427$) under 002 reflection.

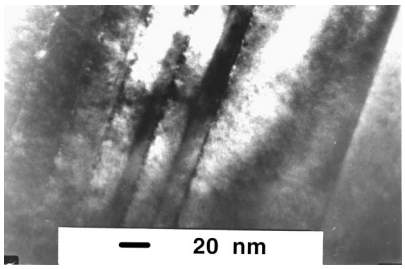

FIG. 3. Cross-section image of sample A2 ($x_{In}=0.427$) under 220.

by the TEM image), as observed from the cross-section micrograph under 002 reflection taken for sample A2 (Fig. 2). From this image, only the thickness of the barriers and the thickest QWs can be estimated with a certain degree of accuracy, being the error of the determination is around ± 1 ML. The estimated barrier thicknesses deviates from nominal values by about 6%, which means an expected deviation around 3% for QW thicknesses (In and Ga cells work during the alloy growth but only the Ga cell works for QWs).

In Fig. 3 the same sample is observed by TEM under the 220 reflection. The image shows that the two QW interfaces are asymmetric, with some kind of roughness in the well/barrier interface (bottom interface, as seen from the buffer layer) while the barrier/well interface (upper interface) remains smooth. The origin of this roughness could be attributed to imperfections in the alloy. A much more clearly developed contrast modulation is observed under 400 and 040 reflections in plan view. Figure 4 shows a micrograph of a single $In_{0.47}Ga_{0.53}P$ layer grown by ALMBE under identical growth conditions. The modulation has a spacing in the range 10–20 nm and is oriented along $\langle 100 \rangle$ directions in the (001) growth plane. The appearance of this fine structure has been ascribed to the existence of compositional fluctuations due to the decomposition of the InGaP alloy in both In- and Ga-enriched regions and/or to alloy disordering effects.[3,11] On the other hand, no traces of long range ordering are observed by electron diffraction and Raman scattering measured on this InGaP single layer sample.[3] Therefore, the InGaP barriers of our QWs should be nominally free from long range ordering effects. Furthermore, Raman scattering has been measured in all samples (not shown here) to control once more the degree of ordering with the same final conclusion.

IV. OPTICAL CHARACTERIZATION

Figure 5 shows the PL spectra of samples A1, A2, and B1. An outstanding feature observed in our InGaP/GaAs QWs is the important energy blueshift of the PL lines [about 60 meV between the 3 ML (0.85 nm) thick QWs] when the In–Ga ratio of the barrier alloy decreases from $x_{In}=0.541$ to

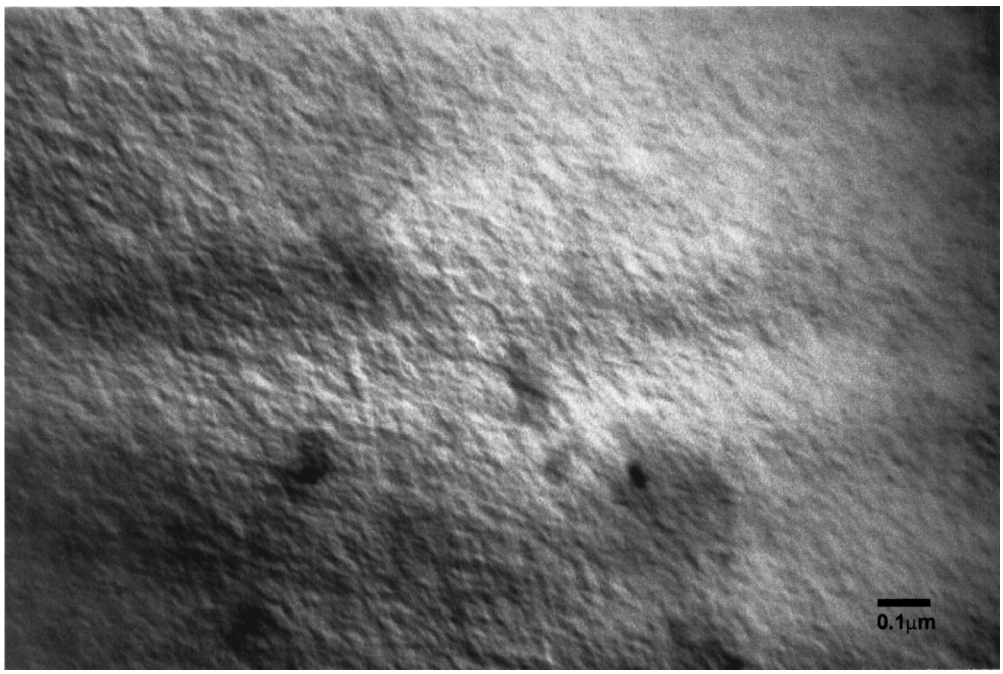

FIG. 4. Plan-view transmission electron micrograph of an InGaP epilayer grown by ALMBE. The In content for this layer is 0.48, i.e., lattice matched to the GaAs (001) substrate. A modulated contrast parallel to the $\langle 010 \rangle$ direction is observed under the 400 reflection.

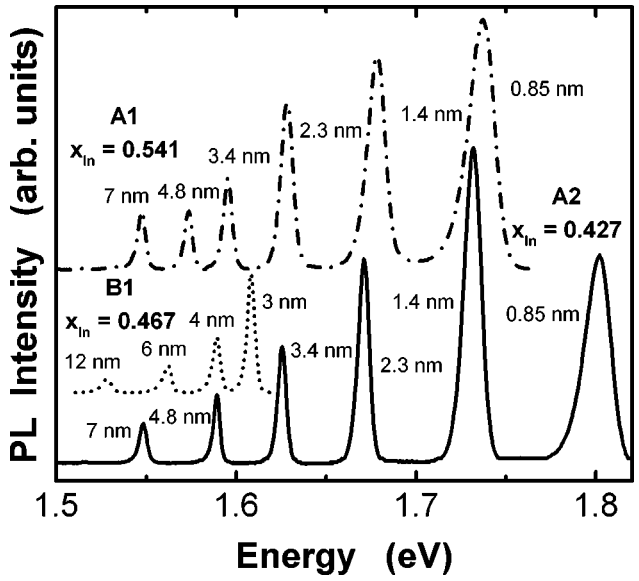

FIG. 5. PL spectra (excitation at 514.5 nm) at 2 K for all samples.

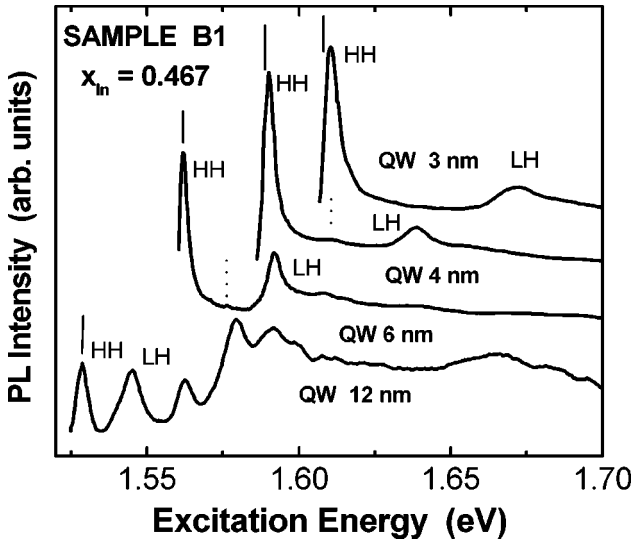

FIG. 6. PLE spectra at 2 K of the different QWs in sample B1 (near lattice matched to GaAs, $x_{In}=0.467$). Short solid lines indicate the position of the PL peak energy (from Fig. 5) and short dotted lines the tentative position of the HH–exciton continuum onset. The detection energies for these spectra are 1.525, 1.561, 1.586, and 1.606 eV, corresponding to the 12, 6, 4, and 3 nm wide QWs, respectively.

$x_{In}=0.427$ [it is strong enough to be explained only by taking into account the increase of the barrier band gap (100–110 meV), as will be discussed below].

The overall optical quality, firstly represented by the PL linewidth in Fig. 5 and the reproducibility achieved in our samples, is quite satisfactory. To our knowledge, no such good quality (considering the whole QW thickness range examined, from 3 to more than 40 ML) has been achieved.[12–16] The good quality achieved in our samples could be due to the growth process itself, because no important exchange reactions take place between P and As during growth by ALMBE at rather low temperatures, leading to an improvement of the InGaP–GaAs interfaces as compared to other epitaxial techniques.

The optical quality of a heterostructure is usually measured by the full width at half maximum (FWHM) of the PL line and the Stokes shift (SS). Figure 6 shows the PLE spectra for all the QWs of sample B1 (InGaP barriers near lattice matched to GaAs). The SS is zero for the 12 and 6 nm thick QWs, less than 1 meV for the 4 nm thick QW and about 2 meV for the 3 nm thick QW. From the point of view of this spectral parameter, the quality of these QWs would be as good as in the best quality AlGaAs/GaAs QWs.[17] However, the FWHM is practically independent of the QW thickness in B-set samples (5–6 meV) and greater than the values one could expect from the measured SS. In relatively good quality AlGaAs/GaAs QWs, the SS is representative of the thermal occupation of the inhomogeneously broadened excitonic levels at carrier quasiequilibrium temperatures higher than the lattice temperature, and the SS becomes proportional to the broadening parameter and inversely proportional to the quasiequilibrium temperature.[17,18] In our InGaP/GaAs QWs this relation seems to apply somehow for thin QWs, but not for the thick ones, where the SS is negligible as compared to the FWHM. Following Ref. 18, a poor thermal equilibrium between excitons localized at different sites throughout the plane of the QW can be inferred. Therefore, this effect in conjunction with the measured large FWHM constitute limiting factors to the optical quality of the thick InGaP/GaAs QWs.

The mechanism producing a large FWHM for thick QWs is thought to be responsible for the absence of light emission from the 20 and 15 nm thick QWs (or not well resolved from the PL of the GaAs substrate) in B and A samples, respectively, as was previously reported for B samples.[8] In that work, a localization dynamics was also noticed for the 12 nm thick QWs: the PL line is redshifted up to 5 meV when decreasing the excitation photon energy below the InGaP band gap [PL peak at 1.523 eV with 803 nm (1.544 eV) excitation; 1.528 eV with green excitation]. That is, the SS depends on the PL excitation energy, being minimum for the above barrier excitation. This effect is lower in the 6 nm wide QW (2 meV redshifted) and negligible in the two thinnest QWs.

If the PL of the thick QWs changes with excitation energy (existence of exciton localization dynamics), one will also expect changes in the PLE spectrum at different detection energies. Two characteristic PLE spectra obtained by changing detection energy from lower (1.5215 eV) to higher (1.525 eV), are shown in Fig. 7 for the 12 nm wide QW of sample B1. Some extra peaks, namely T1 and T2, cannot be related to the possible optical transitions associated with this QW size (their positions are indicated by dotted lines in Fig. 7). Either transitions from the 20 nm thick QW in this sample or different spatially localized excitons could be assumed as the origin of these extra peaks. The second hypothesis seems more reliable because it is supported by two other experimental facts: (i) the FWHM measured for the HH–exciton resonances in the PLE spectra is narrower than that measured for the PL lines, 4.5 (6.4), 4.4 (5.5), 3.6 (5.2) and 5 (5.1) meV for 12, 6, 4 and 3 nm thick QWs, respectively, and (ii) the HH–exciton continuous onset (and 2s HH–

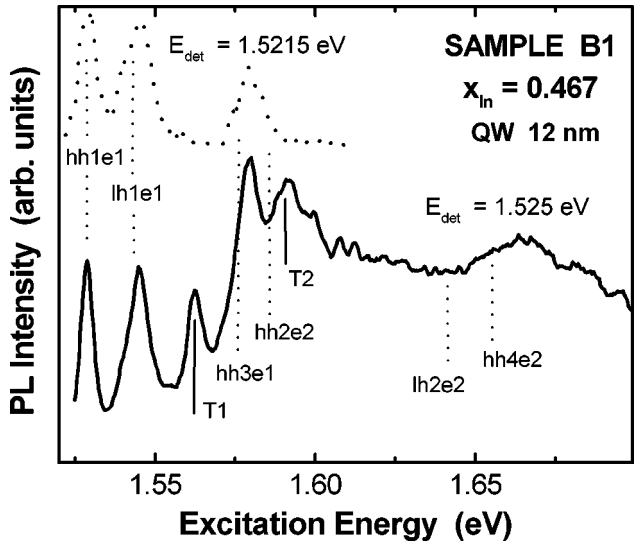

FIG. 7. PLE spectra at 2 K of the 12 nm thick QW of sample B1 ($x_{In}=0.467$) under two different detection energies (indicated in the figure). The possible optical transitions for this QW are indicated by dotted lines; they have been calculated as indicated below for $Q_C=0.13$.

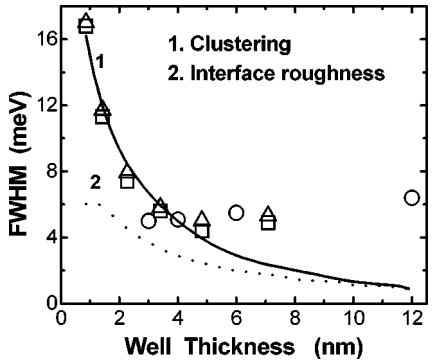

FIG. 9. Measured FWHM in all QWs of the different samples: B1 (hollow circles), A1 (hollow triangles) and A2 (hollow squares). The curves 1 and 2 are related to the estimated contributions [by Eqs. (1) and (2)] from the two most important broadening mechanisms: alloy clustering (curve 1) and interface roughness (curve 2).

exciton resonance) is not resolved between the 1s HH– and LH–exciton transitions of the PLE spectra (somehow a small bump appears in some spectra, which are marked by dotted lines in Fig. 6).

The above given results have demonstrated the existence of an important exciton localization dynamics in thick QWs. We will now try to elucidate its origin. Exciton localization effects occur at spatial zones whose lateral dimensions are comparable to the exciton Bohr radius, when local changes of the confining potential or local fluctuations of the QW thickness take place. We know from Sec. III that both kinds of defects can exist in thick QWs, but we cannot say which is the most important from the data shown up to here. The PLE spectra depicted in Fig. 8 for different QWs of sample A2 give us a surprising result: the photon absorption below the average band gap of the InGaP barriers (2.04 eV) is more and more pronounced for thicker QWs, even giving rise to an additional absorption band. This absorption band cannot be attributed to high energy transitions in the QWs, because it is centered at about the same energy (1.97–1.99 eV) in the three thickest QWs (3.4, 4.8 and 7 nm) its shape is similar and its importance with respect to the average barrier band edge increases when increasing the QW width. The most reliable hypothesis arises from the existence of local compositional fluctuations (fine structure 10–20 nm in size) as discussed in Sec. III for a nearly lattice-matched sample. That absorption band could be associated with a spatial distribution of defect zones—those where the alloy composition is different from the average value. If we translate the energy to In composition, we find that the center energy of that extra absorption band in Fig. 8 nicely corresponds to the lattice-matched alloy $In_{0.48}Ga_{0.52}P$. At the same time, if the preferred alloy composition in these defect zones is around the lattice match value, no such absorption bands should be observed in sample B1. In fact this is the real case for samples B1 and A1—the latter because the absorption in defect zones would be above the average alloy band gap. However, the most important fact affecting the QW optical quality (exciton localization) is not the most probable local composition in defect zones, but its existence. Assuming a Gaussian distribution for these compositional defects, one finds a typical deviation about $\sigma_x=0.04$ for sample A2. In this sense, the PLE of the two widest QWs in sample B1 exhibits a less pronounced and broader barrier band edge than the thinnest one.

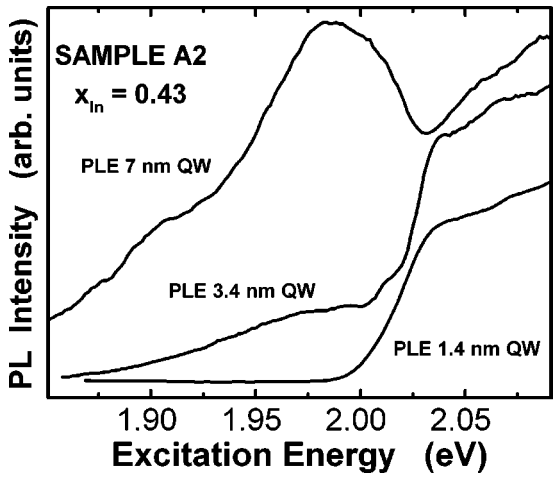

FIG. 8. PLE spectra at 2 K of three QWs in sample A2 ($x_{In}=0.427$) in the energy range of the barrier band edge.

In conclusion, exciton localization effects in thick QWs [excitation (detection) energy dependence of the PL (PLE) and hence a not well defined SS value] should arise from carriers photogenerated at defect zones (the 10–20 nm spaced compositional modulation observed by TEM) where barriers have a significantly different composition (within the Gaussian distribution for these defects). The usual PL–PLE comparison can lead to erroneous conclusions if no further characterization is done.

Figure 9 shows the FWHM measured for the different QWs in the three samples studied here. For QWs thicker than 5 nm the FWHM is not sensitive to the QW width variation (precisely the thickness range where exciton localization ef-

fects dominate as was discussed above). For QWs thinner than 5 nm, the FWHM rapidly increases by decreasing QW width likely to occur in the well known GaAs/AlGaAs system. In this system, interface roughness due to QW width fluctuations is the most important broadening mechanism.[19] In other systems such as InGaAs/InP (or InGaAsP/InP) QWs near lattice matched to InP substrates (which is the analogous case of InGaP/GaAs on GaAs) compositional fluctuations (clustering) in the alloy are normally taken into account by explaining the PL line broadening.[20,21] The FWHM can be estimated by the expressions:[19–21]

$$\Delta E_C = 2.355 \left| \frac{\partial E_{\mathrm{QW}}}{\partial x} \right|_x \left\{ 0.327 \left[x(1-x) \frac{R_C^3}{R_X^3} \right]^{1/2} \right\}, \tag{1}$$

$$\Delta E_R = 2.355 \left| \frac{\partial E_{\mathrm{QW}}}{\partial L_W} \right| \delta L_W, \tag{2}$$

$$\mathrm{FWHM} = (\Delta E_C^2 + \Delta E_R^2)^{1/2}, \tag{3}$$

where C stands for clustering and R stands for interface roughness, L_w is the QW width, x is the In composition in the alloy (we have used the lattice match value, 0.48), E_{QW} is the calculated confinement energy (as given below), and R_C and R_X are the cluster and exciton radii, respectively. Curve 1 (continuous line in Fig. 9) represents the calculated values of Eq. (1), considering R_X to be nearly constant (exciton calculations are out of the scope of this paper).[19] A cluster radius of 0.15 R_X (where the magnitude is similar to that found for InGaAs/InP QWs[20]) has been chosen as the value (the maximum one) which reproduces experimental results in the thickness range below 5 nm. Curve 2 (dotted line in Fig. 9) is the interface roughness contribution given by Eq. (2) by considering $\delta L_w = 0.015 L_w$—that is, half the thickness deviation (two interfaces) from nominal values estimated in Sec. III. Equation (3) yields approximately the same curve as Eq. (2) (the largest value dominates) after an appropriate change of both parameters R_C and δL_w. A reasonable agreement to experimental data is found for R_C in the range $(0.10-0.15)R_X$ and δL_w below 2.5% of L_w. These limits do not differ appreciably if the average composition used for the calculation of confinement energies (and derivatives) is that of samples A1 or A2.

The above evaluation of the FWHM, even though considered as a rough estimate, is in qualitative agreement with structural results related to rather smooth interfaces. Short size alloy clustering (close to the value $R_C \sim 1-1.5$ nm) should also be considered as an important broadening mechanism for thin QWs. On the other hand, if one does an estimate of R_C for reproducing the large FWHM measured in the 12 nm wide QW, a value close to R_X will be found. Such a large R_C value is consistent with the 10–20 nm compositional modulation size, which was assumed above to be responsible of the observed exciton localization effects. It is obvious that Eq. (1) would predict huge FWHM values for thin QWs if this large size R_C was maintained for all QW widths; that is, Eq. (1) does not contemplate exciton localization at the clusters. In thin QWs the exciton radius will become smaller [increase of the two-dimensional (2D) confinement] than the large size clusters and shorter size clustering of the alloy arises as the dominant broadening mechanism of the PL line. The effect of large size compositional modulation on thin QWs can be seen as an additional lateral confinement, similar to that observed in QWs grown on vicinal surfaces.[22]

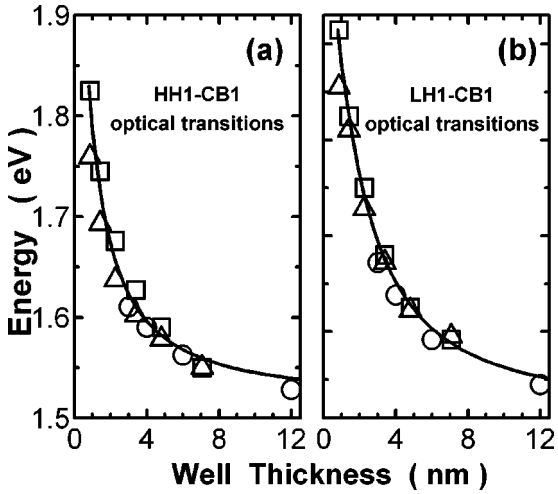

FIG. 10. Summary of the (a) HH– and (b) LH–exciton related optical transition energies measured in all QWs of the different samples (the same symbols as in Fig. 9 are used). Continuous lines represent the calculated energy (for $x_{\mathrm{In}} = 0.48$) as a function of the QW width for HH and LH optical transitions.

After the discussion of optical quality of our samples, we can now deal with more intrinsic optical properties of the $In_xGa_{1-x}P/GaAs$ QWs following our previous investigation in B samples.[8] In that work, the effect of a change in the alloy In–Ga ratio around the lattice match composition was studied for the first time; x_{In} values ranged from 0.45 to 0.51. An increase of the conduction band offset from compressive ($x_{\mathrm{In}} > 0.48$) to tensile strain ($x_{\mathrm{In}} < 0.48$) samples was reasonably assumed to account for the observed blueshift in their corresponding optical transitions. Looking for a stronger corroboration, A samples were grown by expanding the In–Ga ratio and the QW width range. Once again, an important blueshift has been observed from sample A1, $x_{\mathrm{In}} = 0.541$ (compressive strain) to sample A2, $x_{\mathrm{In}} = 0.427$ (tensile strain) as was shown in Fig. 5. The structural and optical characterization performed on B and A samples make us now more confident about the intrinsic nature of such a blueshift, disregarding error sources like uncertainties in the QW width or the barrier composition along the growth direction.

Figure 10 summarizes the observed optical transitions in the different samples. In this work we have taken a value of $Q_C = \Delta E_C / \Delta E_g = 0.13$ for $x_{\mathrm{In}} = 0.48$, following our previous findings.[8] This value of Q_C coincides with that obtained by Chen *et al.*[23] However, the band offset of the InGaP/GaAs system is still a controversial subject, and a wide range of values can be found in the literature (see for example, the most recent works of Refs. 9 and 24 and other references therein). The different content of ordered $GaInP_2$ domains in different samples can be a possible origin for such a great divergence, because a type II alignment between fully ordered $GaInP_2$ and GaAs has been predicted by Froyen *et al.*[9]

In this sense, the effective band offset of the InGaP/GaAs system should decrease when reducing the content of ordered domains in the alloy. At this point, we are able to give some basic facts in favor of a low value of Q_C (as the value proposed by us, Froyen *et al.*[9] and Chen *et al.*[23]):

(i) Only HH– and LH–exciton optical transitions are observed for QWs thinner than about 6 nm. This is not the case for the well known AlGaAs/GaAs system (Q_C about 0.6).

(ii) The energy difference between HH– and LH–exciton transitions gradually increases by reducing QW width up to more than 100 meV for the thinnest QWs, never measured in the AlGaAs/GaAs system (similar hole effective masses and band gap difference).

(iii) The well width dependence of the HH– and LH–exciton optical transition energies is reasonably reproduced by using the band gap offset $Q_C=0.13$, as observed in Fig. 10 (continuous line).

This calculation has been made considering the experimental band gap energy of the near lattice match InGaP barriers in sample B (by PLE) and the most used values (from those reported in the literature) for electron HH and LH masses: $m_e^*=0.12m_0$, $m_{\mathrm{HH}}^*=0.47m_0$, and $m_{\mathrm{LH}}=0.145m_0$, respectively. Exciton correction has not been taken into account, which is the reason for the eventual better agreement with the experimental optical transitions observed in sample A2.

In spite of the reasonably good agreement between the experiment and our estimate for both HH– and LH–exciton optical transitions, the absolute energy blueshift between the transitions in sample A1 and those in A2 cannot be as easily reproduced by only considering the increment of the alloy band gap from $x_{\mathrm{In}}=0.541$ to $x_{\mathrm{In}}=0.427$ (from PLE measurements: 1.935–2.035 eV) keeping the band alignment $Q_C=0.13$ constant. In this case, the HH (LH) potential barrier will increase from compressive to tensile strain by about 125 meV (50 meV) whereas the electron potential barrier only changes by 13 meV.

Here it is interesting to point out some details about the calculation. We have extended the model by Chuang[25] to the case of strained barriers using experimental values for their band gap and LH–HH splitting (well resolved in the PLE spectra of the thinner QWs for each sample).

We have taken, as the best working formula, $V_e=Q_C\Delta E_g$ and $V_{\mathrm{HH(LH)}}=(1-Q_C)\Delta E_g+(-)\delta$ (in the case of tensile strain; opposite signs for compressive strain) for the different carrier potential barriers, where δ is half the splitting between LH– and HH–exciton transitions in the InGaP barrier, and ΔE_g is the energy difference between the InGaP strained (hydrostatic) band gap and that of the GaAs. It is really difficult to match the well width dependence for both HH– and LH–exciton transitions by using the procedure referred to by Chuang[25] (it needs the knowledge of the unstrained band gap, and the deformation and shear potentials): first applying the band offset between the unstrained materials and adding the calculated uniaxial and hydrostatic energy shifts later (the last divided for conduction and valence bands by using the 2/3–1/3 rule, respectively).

The scale imposed by the optical transitions summarized in Fig. 10 is not the best one to highlight the energy changes when tuning the In composition around the lattice match value. Figure 11(a) details the energy blueshift from sample A1 ($x_{\mathrm{In}}=0.541$) to A2 ($x_{\mathrm{In}}=0.427$) for HH– (solid circles) and LH–exciton (solid triangles) transitions. Figure 11(b) shows the LH–HH energy difference, $\Delta E_{\mathrm{LH-HH}}$, for samples A1 (hollow squares) and A2 (solid squares). We have calculated the subband energies for all kinds of carriers as a function of the QW width for samples A1 and A2 under two conditions: (1) $Q_C=0.13$ and (2) Q_C varies about 30% around the lattice match value; that is, $Q_C=0.09$ is used for sample A1 (InGaP under compressive strain) and $Q_C=0.17$ for sample A2 (InGaP under tensile strain).

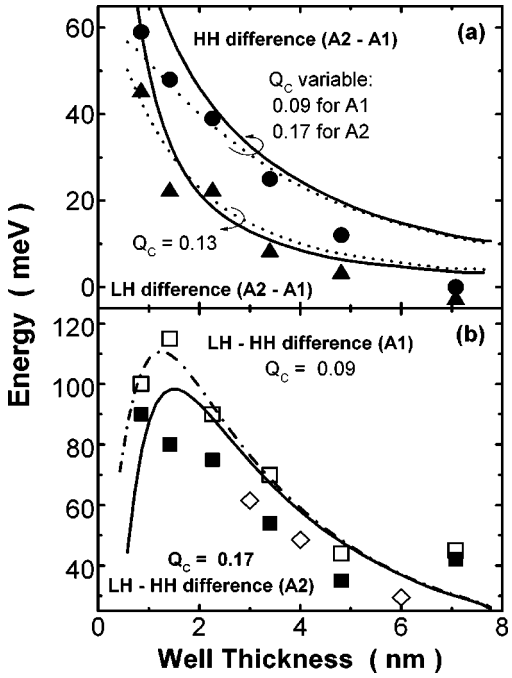

FIG. 11. Compositional and strain effects on the valence band states: (a) blueshift between samples A1 and A2 for HH excitons (solid circles) and LH excitons (solid triangles), and (b) energy difference between HH and LH excitons for samples A1 (hollow squares), A2 (solid squares) and B1 (hollow diamonds).

Before the comparison between calculated and experimental values in Fig. 11, we note that the experimental HH (LH) blueshift in Fig. 11(a) contains the difference between the associated exciton binding energies under tensile (T) and compressive (C) strain, $E_b^{\mathrm{HH(LH)}}(T)-E_b^{\mathrm{HH(LH)}}(C)$. Moreover, the energy difference between both series of experimental points [in Figs. 11(a) and 11(b)], is the same: $(E_b^{\mathrm{HH}}-E_b^{\mathrm{LH}})\times(T)-(E_b^{\mathrm{HH}}-E_b^{\mathrm{LH}})(C)$.

It is striking that excitons confined in GaAs are so sensitive to the relatively slight strain change in the alloy, even if this effect is enhanced because we pass from compressive to tensile strain conditions: the blueshift found for HH excitons is 15–20 meV larger than for LH excitons in QWs thinner than 3.5 nm. Without taking into account the barrier strain state, the exciton binding energy could only vary around 2 meV for the measured 120 meV increase of the barrier band gap, as occurs for the AlGaAs/GaAs system.[26] In this way, we would expect a similar QW width depen-

dence for HH and LH blueshifts (as in our calculated curves without exciton correction). The observation of such a huge difference between HH and LH excitons blueshifts can be related to the small value of Q_C, which implies huge valence band potential barriers and thus both 2D exciton wave function and binding energy—mostly determined by holes.

Condition (1), $Q_C=0.13$, predicts the correct blueshift for the HH and LH optical transition in the 0.85 nm thick QW, but the well width dependence of the HH blueshift [bottom continuous line in Fig. 11(a)] exhibits a rapid decrease and clearly underestimates the other measured values. On the other hand, the calculated curve for the LH blueshift [bottom dotted line in Fig. 11(a)] agrees with experimental values in the whole range. In condition (2), Q_C variable (30%), both calculated blueshift curves for HH and LH [upper continuous and dotted lines in Fig. 11(a), respectively] predict a slower decrease with well width, and the experimental HH blueshift in the whole QW width range would be reasonably reproduced. Therefore, taking into account the considerations given above concerning the effect of strain on the exciton binding energy, a variation in Q_C of at least $\approx$15% and maximum $\approx$30% from compressive ($x_{\mathrm{In}}=0.541$) to tensile ($x_{\mathrm{In}}=0.427$)strained barriers will be reasonably expected. This percentage will be closer to 30% as the binding energy for the LH excitons is more sensitive to the change from compressive to tensile strain conditions in the barrier, which probably is the case. In Ref. 8 a larger percentage was deduced, because the estimate was only done on the basis of the HH blueshift observed in the 3 nm QW, without realizing the different effects of strain on exciton confinement.

Finally, the calculated well width dependence of the LH-HH energy difference is compatible with the measured values [Fig. 11(b)] under both conditions for Q_C (disregarding the excitonic shift between samples A1 and A2, as discussed above). The reason is that condition (2) also takes $Q_C=0.13$ as the central value when passing from compressive ($Q_C=0.09$) to tensile ($Q_C=0.17$) strain conditions. Larger (lower) values for the central Q_C would reduce (increase) appreciably the calculated LH-HH energy difference. The main difference between conditions (1) and (2) arises in the QW width region below 2 nm, because of the saturation in the LH subband energy. We obtain a greater difference in this region by using a variable Q_C value than a constant value (practically negligible, and not shown for clarity), which seems closer to the tendency exhibited by the experimental data [Fig. 11(b)] (even if the HH–exciton energies for the three thinnest QWs are less accurate due to the large SS and line broadening).

V. CONCLUSIONS

In summary, our results show that high quality InGaP/GaAs QWs have been grown in a wide range of thicknesses at low substrate temperatures by ALMBE. Measurable Stokes shifts in thin QWs ($<$4 nm) and broad FWHM (5–6 meV) of the PL emission lines from thicker QWs (limiting factors of the optical quality of our InGaP/GaAs QWs system) can be explained by exciton localization effects due to potential fluctuations in the InGaP barriers produced by alloy disordering. Spatial localization at zones with different compositions (10–20 nm in size) has a stronger effect on thick QWs. An important blueshift in the PL lines of the GaAs QWs ($\cong$60 meV for 0.85 nm thick QWs) is observed when changing the composition of the barrier alloy from $In_{0.541}Ga_{0.459}P$ (compressive strain) to $In_{0.427}Ga_{0.573}P$ (tensile strain). This result has been explained by an increase of the conduction band offset from compressive to tensile strained barriers in the InGaP/GaAs QW system from $Q_C=0.09$ to $Q_C=0.17$ (maximum difference). The exciton binding energy has to be taken into account for a more conclusive and quantitative analysis, given the important effect of the barrier strain condition (relatively small) on this magnitude. Our results show that the alloy composition of the InGaP barriers is an important parameter for device design.

ACKNOWLEDGMENTS

The authors wish to acknowledge Dr. Carmen Quintana for her help in the TEM work. Thanks are also due to Dr. Yolanda González for her useful participation in the x-ray work. Part of the TEM studies were carried out at the electron microscopy facilities of the Universidad de Cádiz. The first author (J.M.-P.) wishes to acknowledge the French–Spanish cooperation Project No. HF1995-0028. This work was supported by the Spanish ''CICYT'' under Project No. TIC96-1020.

[1] M. C. DeLong, D. J. Mowbray, R. A. Hogg, M. S. Skolnick, M. Hopkinson, J. P. R. David, P. C. Taylor, S. R. Kurtz, and J. M. Olson, J. Appl. Phys. **73**, 5163 (1993).
[2] D. M. Follstaedt, R. P. Schneider, and E. D. Jones, J. Appl. Phys. **77**, 3077 (1995).
[3] L. González, Y. González, G. Aragón, M. J. Castro, M. L. Dotor, and D. J. Dunstan, J. Appl. Phys. **80**, 3327 (1996); L. González, Y. González, M. L. Dotor, and J. Martínez-Pastor, Appl. Phys. Lett. **72**, 2595 (1998).
[4] M. D. Dawson, G. Duggan, and D. J. Arent, Phys. Rev. B **51**, 17660 (1995).
[5] C. Jelen, S. Slivken, X. G. He, M. Razeghi, and S. Shastry, J. Vac. Sci. Technol. B **12**, 1113 (1994).
[6] M. Jalonen, M. Toivonen, P. Savolainen, J. Köngäs, and M. Pessa, Appl. Phys. Lett. **71**, 479 (1997).
[7] K. A. Bertness, S. R. Kurtz, D. J. Friedman, A. E. Kibbler, C. Kramer, and J. M. Olson, Appl. Phys. Lett. **65**, 989 (1994).
[8] J. Martínez-Pastor, L. González, and Ph. Roussignol, Appl. Phys. Lett. **68**, 2111 (1996).
[9] S. Froyen, A. Zunger, and A. Mascarenhas, Appl. Phys. Lett. **68**, 2852 (1996).
[10] J. Zeman, G. Martinez, P. Y. Yu, and K. Uchida, Phys. Rev. B **55**, R13428 (1997).
[11] J. P. Gowers, Appl. Phys. A: Solids Surf. **31**, 23 (1983).
[12] M. J. Hafich, J. H. Quigley, R. E. Owens, G. Y. Robinson, D. Li, and N. Otsuka, Appl. Phys. Lett. **54**, 2686 (1989).
[13] F. Omnes and M. Razeghi, Appl. Phys. Lett. **59**, 1034 (1991).
[14] Ph. Maurel, Ph. Bove, J. C. García, and C. Grattepain, Semicond. Sci. Technol. **6**, 254 (1991).
[15] D. J. Mowbray, O. P. Kowalski, M. S. Skolnick, M. C. DeLong, M. Hopkinson, J. P. R. David, and A. G. Cullis, J. Appl. Phys. **75**, 2029 (1994).
[16] W. Seifert, N. Carlsson, M.-E. Pistol, and L. Samuelson, J. Cryst. Growth **145**, 758 (1994).
[17] M. Gurioli, J. Martínez-Pastor, A. Vinattieri, and M. Colocci, Solid State Commun. **91**, 931 (1994).
[18] M. Gurioli, A. Vinattieri, J. Martínez-Pastor, and M. Colocci, Phys. Rev. B **50**, 11817 (1994).
[19] M. A. Herman, D. Bimberg, and J. Christen, J. Appl. Phys. **70**, R1 (1991).

[20] M. Engel, R. K. Bauer, D. Bimberg, D. Grützmacher, and H. Jürgensen, J. Cryst. Growth **93**, 359 (1988).
[21] M. Sugawara, T. Fujii, S. Yamazaki, and K. Nakajima, Phys. Rev. B **44**, 1782 (1991).
[22] J. Martínez-Pastor, F. Agulló-Rueda, A. Vinattieri, F. Messeguer, J. Sánchez-Dehasa, M. Colocci, R. Mayoral, A. Marti-Ceschin, N. Grandjean, and J. Massies, Superlattices Microstruct. **14**, 39 (1993).
[23] J. Chen, J. R. Sites, I. L. Spain, M. J. Hafich, and G. Y. Robinson, Appl. Phys. Lett. **58**, 744 (1991).
[24] M. S. Faleh, J. Tasselli, J. P. Bailbe, and A. Marty, Appl. Phys. Lett. **69**, 1288 (1996).
[25] S. L. Chuang, Phys. Rev. B **43**, 9649 (1991).
[26] M. Gurioli, J. Martínez-Pastor, M. Colocci, A. Bosacchi, S. Franchi, and L. C. Andreani, Phys. Rev. B **47**, 15755 (1993).